Bioactive Materials 33 (2024) 71–84

Contents lists available at ScienceDirect

Bioactive Materials

journal homepage: www.keaipublishing.com/en/journals/bioactive-materials

An olsalazine nanoneedle-embedded inulin hydrogel reshapes intestinal homeostasis in inflammatory bowel disease

Zhuangzhuang Zhang [a,1], Yang Pan [a,1], Zhaoyuan Guo [a], Xi Fan [a], Qingqing Pan [b], Wenxia Gao [c], Kui Luo [d], Yuji Pu [a,*], Bin He [a,**]

[a] National Engineering Research Center for Biomaterials, College of Biomedical Engineering, Sichuan University, Chengdu, 610064, China
[b] School of Preclinical Medicine, Chengdu University, Chengdu, 610106, China
[c] College of Chemistry & Materials Engineering, Wenzhou University, Wenzhou, 325027, China
[d] Huaxi MR Research Center (HMRRC), Department of Radiology, West China Hospital, Functional and Molecular Imaging Key Laboratory of Sichuan Province, Sichuan University, China

ARTICLE INFO

Keywords:
Inflammatory bowel disease
Intestinal homeostasis
Olsalazine
Hydrogel
Nanoneedle

ABSTRACT

Inflammatory bowel disease (IBD) is a chronic and refractory condition characterized by disrupted epithelial barrier, dysregulated immune balance, and altered gut microbiota. Nano-enabled interventions for restoring gut homeostasis have the potential to alleviate inflammation in IBD. Herein, we developed a combination of olsalazine (Olsa)-based nanoneedles and microbiota-regulating inulin gel to reshape intestinal homeostasis and relieve inflammation. The Olsa-derived nanoneedles exhibited reactive oxygen species scavenging ability and anti-inflammatory effects in lipopolysaccharide-simulated macrophages. The composite of nanoneedles and inulin gel (Cu_2(Olsa)/Gel) displayed a macroporous structure, improved bio-adhesion, and enhanced colon retention after oral administration. Mechanistically, the composite effectively downregulated pro-inflammatory cytokine levels and promoted epithelial barrier repair through anti-inflammatory and antioxidant therapies, resulting in significant alleviation of colitis in three animal models of IBD. Furthermore, analysis of gut microbiota revealed that Cu_2(Olsa)/Gel treatment increased the diversity of intestinal microflora and decreased the relative abundance of pathogenic bacteria such as *Proteobacteria*. Overall, this study provides a self-delivering nanodrug and dietary fiber hydrogel composite for IBD therapy, offering an efficient approach to restore intestinal homeostasis.

1. Introduction

Inflammatory bowel disease (IBD), comprising ulcerative colitis (UC) and Crohn's disease (CD), is a recurrent and refractory disorder with growing public health concern worldwide [1]. The disorder is characterized by dysregulated intestinal homeostasis, which involves damage to the epithelial barrier, immune response disorder, and gut dysbiosis [2,3]. Current clinically approved IBD treatments primarily consist of anti-inflammatory or immunosuppressive agents, aiming to alleviate the immune response. However, these drugs face significant drawbacks due to untargeted drug delivery, leading to side effects like hepatotoxicity, systemic immune suppression, and flare-ups following long-term administration. Therefore, there is an urgent need for nanoscale drug delivery systems that specifically target the colon and/or inflammation sites to enhance local therapeutic levels while minimizing off-target toxicity [4]. Furthermore, recent studies have explored the use of anti-oxidant natural small molecules [5], proteins [6,7] and synthetic inorganic [8–10] and polymeric [11,12] nanomaterials to regulate immune balance, offering a promising anti-oxidation therapeutic strategy for IBD management. Among these approaches, metal-organic frameworks (MOFs) based on various transition metals (Mn [8,13], Ce [14], Ru [15], etc.) have gained attention due to their inherent ROS-scavenging abilities. However, these MOFs typically employ bio-inert organic ligands, and the utilization of bioactive linkers similar

Peer review under responsibility of KeAi Communications Co., Ltd.
* Corresponding author.
** Corresponding author.
E-mail addresses: yjpu@scu.edu.cn (Y. Pu), bhe@scu.edu.cn (B. He).
[1] These authors contributed equally to this work.

https://doi.org/10.1016/j.bioactmat.2023.10.028
Received 5 August 2023; Received in revised form 7 October 2023; Accepted 27 October 2023

to approved IBD drugs is still limited.

Growing data evidence that gut microbiota plays an important role in gut homeostasis and dysbiosis [16], and altered metabolites of microbial communities are associated with the initiation and development of IBD. Microbiome regulation facilitates the mucosa immune homeostasis and intestinal epithelium barrier repair by changing the composition and the metabolites of microbiota, which also interacts with the mucosa immune system. Compared with fecal transplantation and probiotics, leveraging dietary and prebiotics to modulate gut microbiota is safe and low-cost, and could have an impact on a broad-spectrum microorganism [17,18]. Noteworthily, monotherapy is difficult to realize a comprehensive restoration of intestinal homeostasis and maintain a long-standing remission. In addition, oral drugs are challenged by the complicated and harsh physiochemical environments in gastrointestinal tract such as enzymes, bacteria, different pHs, and accelerated intestinal motility. Therefore, it is highly desirable to design an oral bio-adhesive platform that is able to regulate immune response and gut microbiota for a potent therapy of IBD.

In this study, we developed an olsalazine (Olsa)-based nanoneedle/inulin gel composite with an intestinal homeostasis modulating effect for treating IBD (Scheme 1). Olsa, a clinical anti-colitis drug, was used as an organic linker to construct a MOF nanoneedle, which, to our best knowledge, is the first time reported by a facile hydrothermal synthesis method. The Cu_2(Olsa) nanoneedle is not only a Olsa depot but also ROS-scavenging and anti-inflammatory nanomedicine. Moreover, Cu_2(Olsa) nanoneedle has a high surface area to volume ratio, which can increase the drug loading and release time [19]. Compared with other nanoparticles, nanoneedles have the advantage of penetrating the cell membrane and delivering drugs directly into the cytoplasm or the nucleus, thus enhancing the bioavailability and targeting of drugs. In addition, inulin gel was employed to not only increase the bio-adhesion and prolong colon retention but also regulate gut microbiota since that inulin, as a generally recognized as safe (GRAS) reagent, can be only degraded by colonic inulinase and its fermentation by gut microbiota could enrich the diversity and richness of commensal bacteria. Upon oral administration, the macroporous composite could fulfill improved colon adhesion and sustained drug release for anti-oxidation and anti-inflammation treatment, which together with immune and microbiota regulation restored intestinal homeostasis. Our results verified the significant colitis alleviation efficacy of this composite in dextran sulfate sodium (DSS) and 2,4,6-trinitrobenzene sulfonic acid (TNBS)-induced UC and CD animal models. This study provides a simple and robust bioMOF/hydrogel composite platform with efficient colonic drug delivery and minor safety concerns for reshaping intestinal homeostasis, holding a potential in the treatment of IBD and other disorders that are closely correlated with intestinal homeostasis.

2. Results and discussion

2.1. Design, synthesis, and characterization of Cu_2(Olsa) MOF nanoneedle

In this study, we selected Olsa as the organic linker for nanoMOF synthesis. Olsa was chosen due to its clinical application in treating IBD and its symmetrical chemical structure, which possesses two carboxyl groups capable of coordinating with transition metal ions to form diverse nanoscale MOFs. Moreover, the azo bond within Olsa can be enzymatically cleaved by bacterial azoreductase in the colon, resulting in the production of two molecules of 5-aminosalicylic acid (5-ASA), an active anti-inflammatory agent. To further improve the colon retention of Olsa-based nanoMOFs and regulate gut microbiota, we designed a Olsa-based MOF/inulin gel composite for IBD treatment. Inulin, a natural linear fructan extracted from various edible plants, was chosen as the polysaccharide for constructing the hydrogel due to its advantageous properties. First, inulin exhibits high biocompatibility and safety for biomedical applications. Second, the presence of abundant hydroxyl groups in inulin allows for robust crosslinking and formation of hydrogels, which could enhance bioadhesion and colonic retention. Third, inulin, as a prebiotic fiber, is enzymatically degradable by inulinase found in the colon and the metabolites could stimulate the growth of beneficial *Bifidobacterium* and *Lactobacillus* in the gut microbiota.

Cu_2(Olsa) MOFs were readily prepared by a hydrothermal method owing to the great water solubility of $CuCl_2$ and sodium olsalazine (Olsa). We first studied the impact of reaction temperature on the size and morphology of Cu_2(Olsa) at a feeding Cu/Olsa molar ratio of 2/1, which indicated 70 °C was a moderate temperature (Fig. S1). At this reaction temperature, the growth kinetics revealed that a large number of micron-sized needles were observed at 1 h (Fig. S2) and we chose a reaction time of 12 h for a complete MOF growth in the following studies. As shown in the scanning electron microscopy (SEM) images,

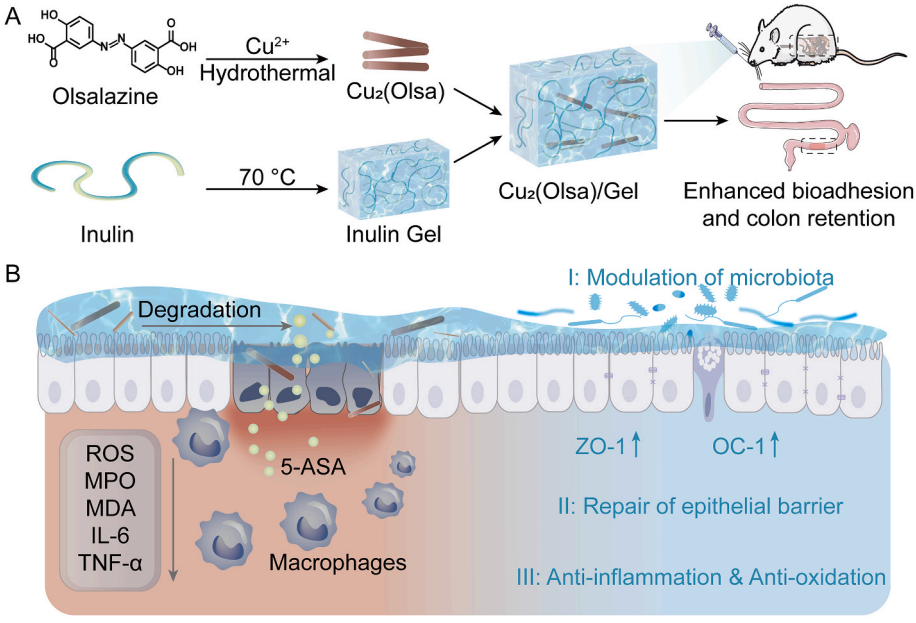

Scheme 1. Schematic illustration of Cu_2(Olsa) and inulin gel composite for IBD treatment by restoring intestinal homeostasis. (A) Preparation of Cu_2(Olsa)/Gel. (B) The proposed therapeutic mechanisms of Cu_2(Olsa)/Gel.

Cu_2(Olsa) prepared at different Cu/Olsa feeding ratios maintained a needle-like morphology except a petaloid morphology at a high Olsa feeding ratio (Cu/Olsa = 1/10) (Fig. 1A and S3); what's more, the MOFs with ratios of 10/1, 8/1, 4/1, 2/1, 1/2, and 1/4 exhibit similar rod-like morphologies with smooth surfaces, besides, the lengths of nanoneedles are in the range 3–7 μm and a comparable width of 0.1 μm when the Cu/Olsa ratio was higher than 1/4 (Fig. 1B and C). However, the MOF with a 1/8 ratio demonstrates a distinct bamboo leaf-like shape, characterized by a curved surface and pointed tip. Most notably, the MOF with the smallest 1/10 ratio forms unique clustered structures resembling flower petals, which might be composed of numerous short bamboo leaf-shaped MOFs aggregated together. These flower petal-shaped structures have an average length of 3.09 μm and width of 0.79 μm. Powder X-ray diffraction (PXRD) results manifested that these MOFs shared the same diffraction peaks but different diffraction intensities (Fig. 1D), suggesting the same coordination geometry but different orientations [20]. Additionally, the more robust coordination bonds along pore channels promote oriented nucleation and growth, yielding macroscopic needle-shaped morphologies. Inductively coupled plasma optical emission spectrometry (ICP-OES) confirmed the presence of copper with a 23.47% in Cu_2(Olsa). A feeding ratio of 2:1 was used in the following study for the atom economy reason (Fig. S4) and the Cu_2(Olsa) prepared at this ratio exhibited a superior ability to scavenge ROS (Fig. 1E). Finally, a weak acidic condition (pH 5.0), which was also close to the pH value of the metal/ligand mixture at a 2:1 M ratio, was determined to be an appropriate pH for the synthesis of needlelike Cu_2(Olsa) (Fig. S5). Together, we successfully prepared micron-sized, needle-like Cu_2(Olsa) using a simple and environment friendly hydrothermal method.

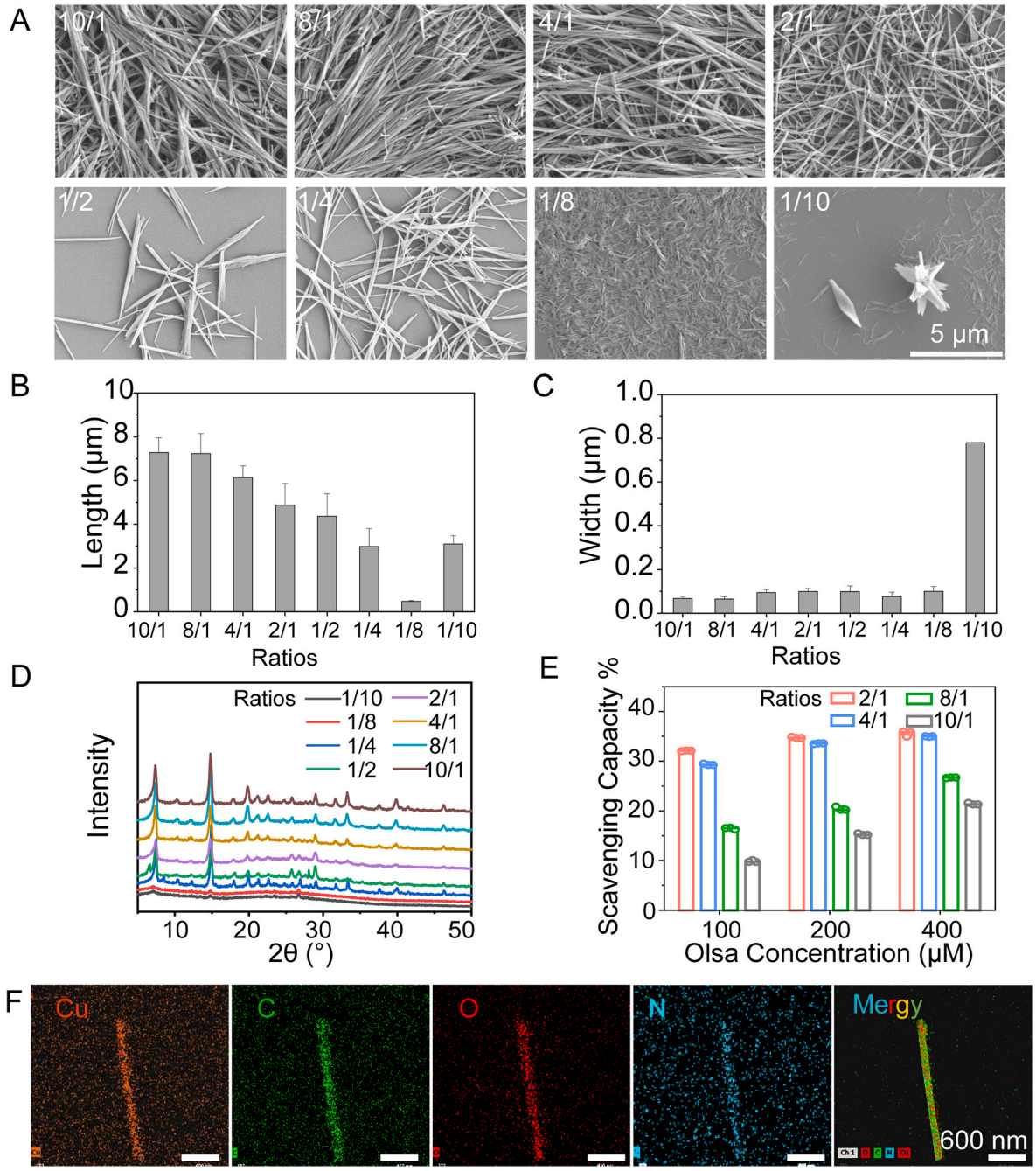

Fig. 1. Characterization of needle-like Cu_2(Olsa). (A) SEM images; (B) lengths, (C) widths, (D) PXRD and (E) $ABTS^{+\bullet}$ scavenging capacity of Cu_2(Olsa) at different Cu/Olsa ratios. (F) Elemental mapping of Cu_2(Olsa) at Cu/Olsa 2/1.

The optimal Cu_2(Olsa) displayed an average length of 5.14 μm and diameter of 0.10 μm as revealed by SEM (Fig. 1A and B). X-ray photoelectron spectroscopy (XPS) was performed to analyze the chemical composition of Cu_2(Olsa). As shown in Fig. S6, the Cu 2p spectra were disassembled into four peaks. The peaks located at ~931.7 and ~952.1 eV indicated the Cu^+ $2p_{3/2}$ and Cu^+ $2p_{1/2}$ spin−orbit doublets in Cu_2(Olsa) [21]. The characteristic peak of Cu(II) at 935.2 eV was also observed, which demonstrated the co-existence of Cu^+ and Cu(II) [22]. The Cu LMM Auger signal was also consistent with the result (Fig. S6). The elemental mapping data from the energy-dispersive X-ray spectroscopy (EDS) demonstrating the homogeneous distribution of C, N, O, and Cu elements (Fig. 1F).

2.2. *In vitro anti-oxidation and anti-inflammation effects of Cu_2(Olsa)*

Next, we investigated whether 5-aminosalicylic acid (5-ASA) can be released from Cu_2(Olsa) in the presence of sodium hydrosulfite, which is a mimic of azoreductase [23]. In the colon tissue, the released Olsa can then be converted to 5-ASA by the colonic bacteria, which can further enhance the anti-inflammatory effect of Cu_2(Olsa). Therefore, the release of 5-ASA from Cu_2(Olsa) is an important indicator of its therapeutic potential for IBD treatment. As shown in Fig. S7A, fluorescence intensities of 5-ASA increased with increasing sodium hydrosulfite concentrations, indicating the hypoxia-responsiveness of Cu_2(Olsa) [24]. The ROS scavenging capacity of Cu_2(Olsa) was also evaluated by 2, 2′-azino-bis(3-ethylbenzothiazoline 6-sulfonate) (ABTS) and 2,2-diphenyl-1-picrylhydrazyl (DPPH) assays [25]. As shown in Figs. S7B and S7C, more than 85% of the $ABTS^{+\bullet}$ could be eliminated upon treatment with 8 mM Cu_2(Olsa) for 30 min. Similarly, 2 mM Cu_2(Olsa) scavenged 40% DPPH at 10 min. Both results suggested that Cu_2(Olsa) could be a potential ROS-scavenger to normalize the ROS level in the inflamed colon. Before the *in vitro* anti-inflammatory study, we first confirmed the cytocompatibility and uptake of Cu_2(Olsa) by macrophages, which are typical infiltrated immune cells at inflamed sites of IBD. As shown in Fig. 2A and B, cell viability was higher than 80% when the Olsa concentration was lower than 250 μM. The efficient cellular uptake of Cu_2(Olsa) by macrophages was confirmed by Bio-TEM (Fig. 2C). It was reported that materials between 250 nm and 3 μm are typically internalized by macrophages through macropinocytosis and phagocytosis [26]. We investigated the uptake of Cu_2(Olsa) by macrophages using Bio-TEM imaging (Fig. 2C). As indicated by the yellow arrows in the figure, the nanoneedles successfully entered the cells. Next, we inspected the *in vitro* anti-inflammatory effect of Cu_2(Olsa) in RAW264.7 cells that were treated with exogenous H_2O_2 (100 μM) to simulate an inflammation environment. Cu_2(Olsa) treatment rescued cells and markedly reduced H_2O_2-induced apoptosis (Fig. 2D, E, and S8). H_2O_2 treatment led to a low cell viability of 58.6%, which could be increased to nearly 100% after co-incubation with 5 μM Cu_2(Olsa). Similarly, H_2O_2 treatment induced a cell apoptosis rate of 24.2% and Cu_2(Olsa) treatment could reduce the apoptosis rate to a basal level (about 7.5%). Furthermore, the anti-inflammatory effect of Cu_2(Olsa) was confirmed by detecting the level of IL-6 mRNA in lipopolysaccharide (LPS)-treated macrophages [27]. As shown in Fig. 2F, compared with the LPS and 5-ASA groups, Cu_2(Olsa) significantly downregulated the intracellular IL-6 mRNA level. Furthermore, Cu_2(Olsa)-enabled intracellular ROS consumption was verified by both confocal laser scanning microscopy (CLSM) and flow cytometry analyses, even if some nanoneedles aggregate into clusters (Fig. 2G and H), where Cu_2(Olsa) treatment normalized the intracellular ROS level of LPS-stimulated macrophages.

Cell migration plays an important role in intestinal ulcer healing [28], and a wound-healing assay was taken to investigate the potential pro-healing effect of Cu_2(Olsa) on the intestinal epithelium (Fig. 2I and J). To minimize the interference effect of cytotoxicity of H_2O_2 in the migration ability of IEC-6 cells, 200 μM exogenous H_2O_2 was used to mimic a pro-inflammatory environment (Fig. S9). Cu_2(Olsa) showed a wound healing area of 90.6%, much higher than that of control group (70.1%). Overall, Cu_2(Olsa) exhibited anti-oxidation, anti-inflammation and pro-healing properties, indicating an enormous potential in IBD treatment.

2.3. *Morphology, injectability, and rheological properties of Cu_2(Olsa)/Gel*

To further improve the colon retention of Olsa-based nanoMOFs and regulate gut microbiota, we designed a Olsa-based MOF/inulin gel composite for IBD treatment by a heating-cooling method (Fig. 3A) [29] and Cu_2(Olsa) was easily incorporated into inulin gel to obtain a Cu_2(Olsa)/Gel composite (Fig. 3B). Inulin, a natural linear fructan extracted from various edible plants, was chosen as the polysaccharide for constructing the hydrogel due to its advantageous properties. First, inulin exhibits high biocompatibility and safety for biomedical applications. Second, the presence of abundant hydroxyl groups in inulin allows for robust crosslinking and formation of hydrogels, which could enhance bioadhesion and colonic retention. Third, inulin, as a prebiotic fiber, is enzymatically degradable by inulinase found in the colon. We further demonstrated *in vitro* that inulin gel still retained the characteristic biodegradability by inulinase (Fig. S10). These gels as well as Olsa-loaded inulin gel (Olsa/Gel) exhibited good injectability for further oral administration (Fig. 3A and B and S11). SEM images revealed that Cu_2(Olsa)/Gel showed interconnected and homogeneous porous structures (Fig. 3B and S12) [30]. Noteworthily, Cu_2(Olsa) nanoneedle was clearly observed in the hydrogel networks of Cu_2(Olsa)/Gel (highlighted by red arrows), suggesting the successful loading without disrupting the nanostructure. Next, the rheological properties of the blank and MOF-embedded hydrogels were compared at different frequencies and strains. As shown in Fig. 3C and D, Cu_2(Olsa)/Gel showed higher loss modulus (G″) than Olsa/Gel and blank inulin gel, suggesting the better viscous property and a potential in pro-longed retention in gastrointestinal tract [29]. In addition, the reversible rheological behavior demonstrated that Cu_2(Olsa)/gel was self-healing (Fig. 3E).

2.4. *In vitro drug release, gastrointestinal retention, and biodistribution of Cu_2(Olsa)/Gel*

Gastrointestinal pH is a challenge for oral formulations and premature release in the upper gastrointestinal tract could increase the systemic exposure and compromise the therapeutic effect of drugs. The *in vitro* drug release behavior of Cu_2(Olsa)/Gel in a gastrointestinal tract simulating condition was studied by using Cu_2(Olsa), Olsa/Gel, and olsalazine sodium as control groups (Fig. 3F). Olsalazine sodium showed a burst release in the simulated intestinal fluid and 71.7% was released at 4 h. However, Cu_2(Olsa), Olsa/Gel, and Cu_2(Olsa)/Gel showed a much slower release at small intestinal pH 5−6 and Olsa released amount was 24.1%, 33.5%, and 20.3%, respectively. These results indicated that MOF structure played an important role in sustained drug release. In addition, an accelerated release at colonic pH 7.4 was observed in all MOF or gel formulations owing to the increased solubility of Olsa. The *in vitro* drug release studies manifested that our MOF/Gel composite enabled sustained and colonic pH-responsive drug release.

Bio-adhesion and retention in colon is pivotal in prolonged drug retention for inflammation remission since the abnormal intestinal motility caused by diarrhea in IBD. A lap-shear adhesion test was carried out to evaluate the bio-adhesion of Cu_2(Olsa)/Gel (Fig. S13) [31]. Interestingly, Cu_2(Olsa)/Gel glued two ribbons of porcine skin tissue porcine skins and withstood a much larger deformation than Olsa/Gel, which could be ascribed to the macroporous structure [32]. The *in vivo* retention study revealed that FITC-labeled inulin gel showed a better colon retention than the solution counterpart (Fig. S14). At 24 h post oral administration, the fluorescence intensity of Gel group at colon tissues was 2.0-fold higher than that of inulin solution. We then investigated the bio-adhesion and retention capability of Cu_2(Olsa)/Gel and Olsa/Gel in DSS-induced colitis mice (Fig. 3G, H and S15).

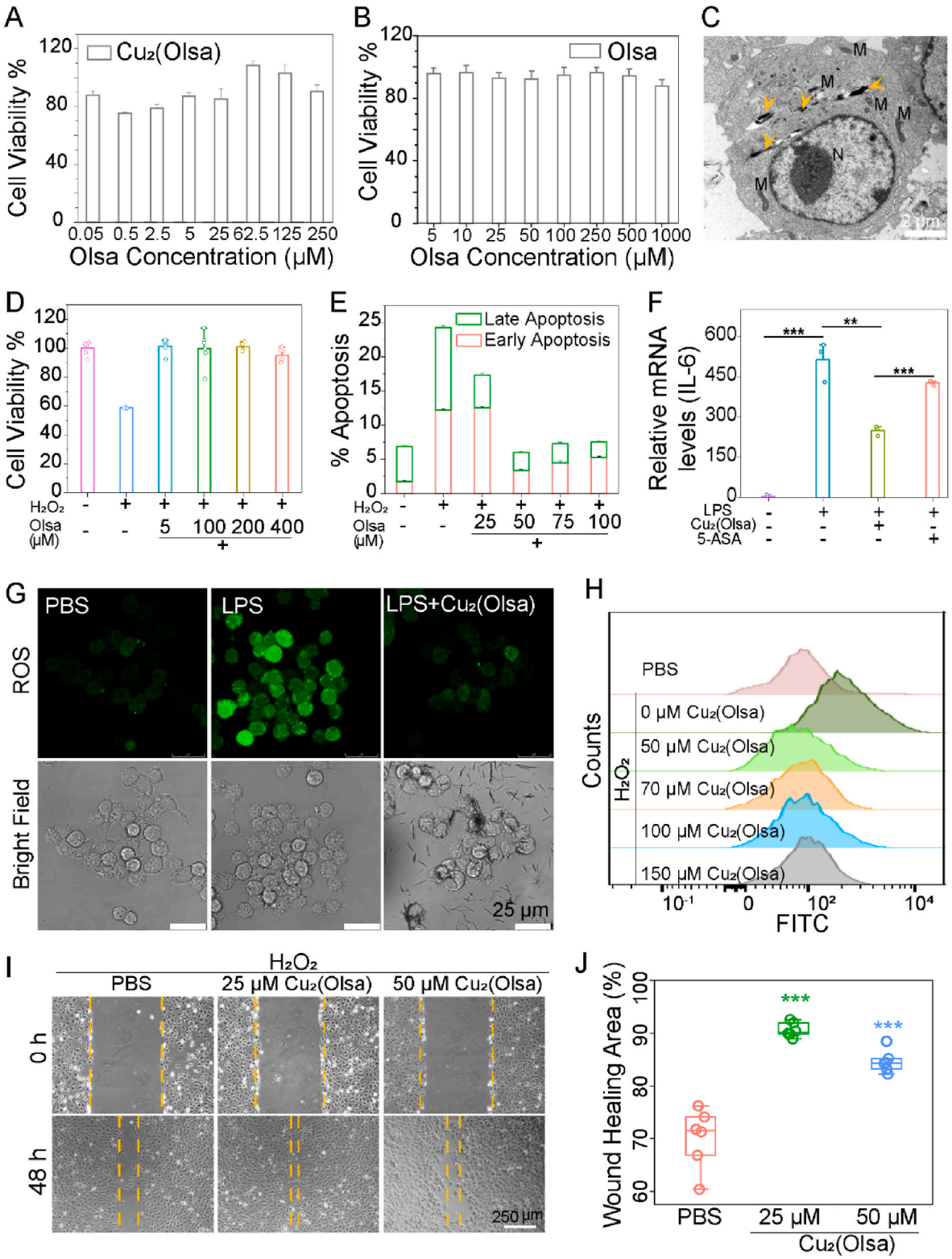

Fig. 2. Cellular uptake and ROS eliminating ability of Cu_2(Olsa). RAW264.7 cell viability of different ligand concentrations of (A) Cu_2(Olsa) and (B) Olsa for 24 h. (C) Bio-TEM image of Cu_2(Olsa)-treated RAW264.7 cells (Nanoneedles were highlighted by yellow arrows; "N" represents nucleus and "M" represents mitochondria). The protective effect of Cu_2(Olsa) in H_2O_2-treated macrophages analyzed (D) by MTT assay and (E) by flow cytometry. (F) The impact of Cu_2(Olsa) and 5-ASA on the IL-6 mRNA levels of LPS-treated RAW264.7 cells. Intracellular ROS level of LPS-treated macrophages determined by (G) CLSM and (H) flow cytometry. (I, J) Wound healing ability of IEC-6 cells treated with PBS or Cu_2(Olsa) at 200 μM H_2O_2. The data are presented as the means ± SE ($n = 3$, $^{**}p < 0.01$, $^{***}p < 0.001$).

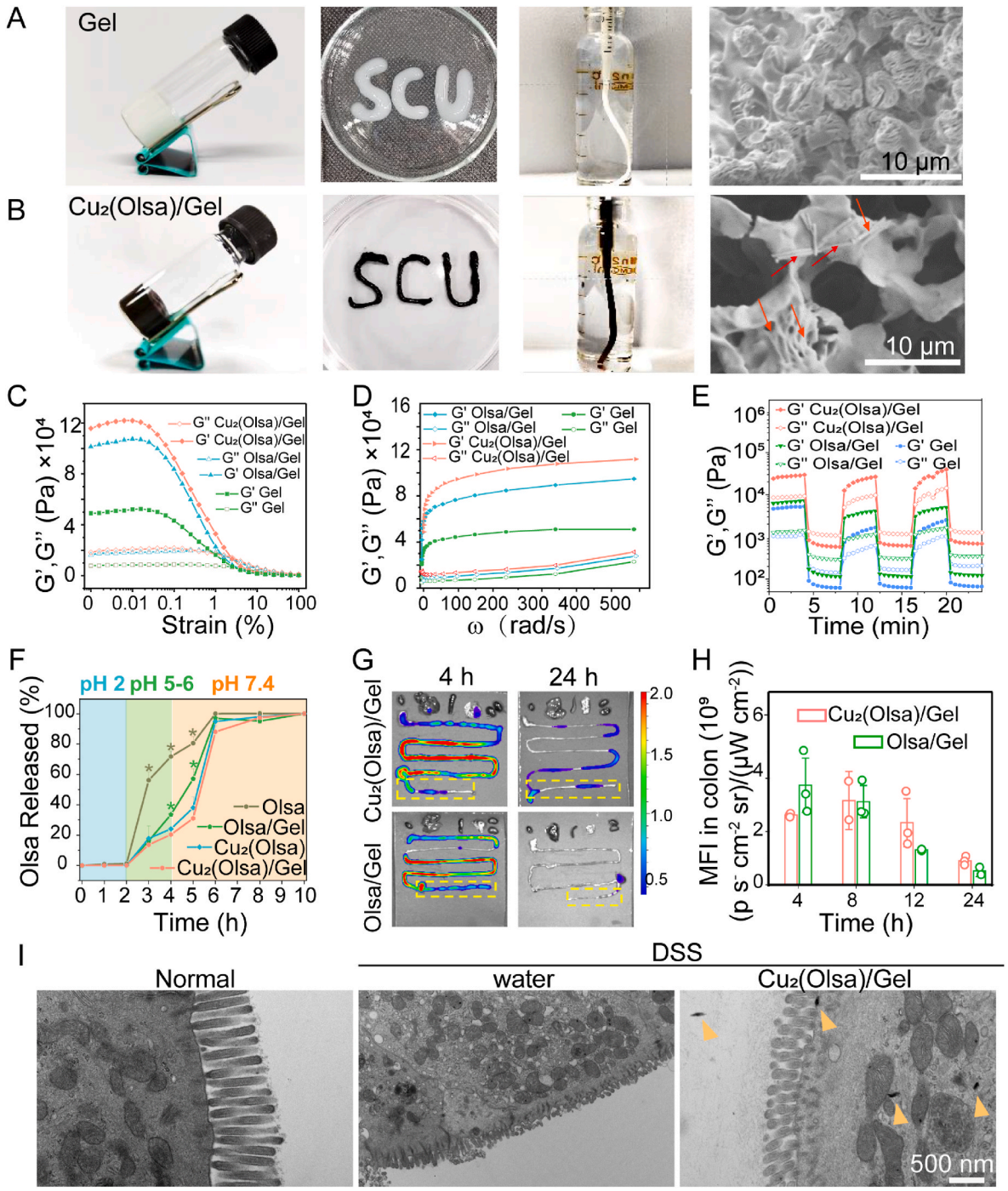

Fig. 3. Characterization of Cu_2(Olsa)-embedded inulin hydrogels. Digital photos, injectability and scanning electron microscopy images of the inulin gel (Gel, A) and Cu_2(Olsa)/Gel (B); red arrows indicate the needle-like Cu_2(Olsa). (C) Amplitude sweep tests of different hydrogel compositions. (D) Frequency sweep tests of the hydrogels. (E) Rheological data of the hydrogel under repeated deformation of 0.1% and 20% strain. (F) In vitro drug release behavior of olsalazine sodium (Olsa), Olsa/Gel, Cu_2(Olsa) and Cu_2(Olsa)/Gel in the gastrointestinal pH conditions ($n = 3$, $^*p < 0.05$, compared with Cu_2(Olsa)/Gel). (G) Typical ex vivo fluorescence images of colon tissues and main organs (from left to right: heart, liver, spleen, lung, kidney) from DSS-treated mice that were intragastric administered Cu_2(Olsa)/Gel or Olsa/Gel (60 mg inulin per dose); (H) the corresponding mean fluorescence intensity (MFI) in the colon at different time points ($n = 3$). (I) Bio-TEM images of the gut lumens of normal and DSS mice; yellow arrows represent Cu_2(Olsa) nanoneedle.

Cu_2(Olsa)/Gel showed a higher fluorescence intensity within 24 h than Olsa/Gel, suggesting the MOF-hydrogel composite displayed an enhanced bio-adhesion and retention effect, which was consistent with the *in vitro* bio-adhesion results. We hypothesize this enhanced adhesion is due to the copper-olsalazine coordination complex, which can increase the mechanical strength and stability of the hydrogel matrix. The reinforced hydrogel network is likely more resistant to shear stress and erosion in the intestinal environment [33]. To further observe the efficient accumulation of Cu_2(Olsa)/Gel at the colonic ulcer sites, we examined the colon by Bio-TEM assay. Fig. 3I shows nanoneedles after degradation by colonic microbes, resulting in shorter nanoneedles, which also demonstrated by the *in vitro* enzymatic reduction reaction assay (~345 nm) (Fig. S16). What's more, Cu_2(Olsa) could efficiently reach colon lumen, enter the colonic epithelial cells, and to some extent

maintain a nanoscale size, which is advantageous for further anti-inflammation/oxidation therapy in IBD. Furthermore, the uptake of Cu_2(Olsa) by intestinal epithelial cells also suggested the biodegradation of inulin gel and subsequent release of Cu_2(Olsa).

2.5. In vivo therapeutic effect and intestinal homeostasis restoration in a delayed therapy of DSS-induced UC model

Intrigued by the anti-inflammatory and colon accumulation advantages, we further evaluated the UC alleviation potential of Cu_2(Olsa)/Gel in a delayed therapy of DSS-induced acute colitis model (Fig. 4A). After a 7 d-induction of colitis, different formulations were orally administrated daily for 7 d. We used Cu_2(dobp)/Gel as a control group since dobp has a similar structure to Olsa but does not have an azo moiety nor known biological functions. Cu_2(dobp) was prepared by the same hydrothermal method and displayed a similar needle morphology to Cu_2(Olsa) and had a slightly increased length of 5.64 μm (Fig. S17A). Cu_2(dobp) maintained highly consistent with the dimensions and crystal structure of Cu_2(Olsa) owing to their similar ligand structures (Fig. S17B). On day 14, body weights of 21.35 g and 20.87 g were observed for the Cu_2(Olsa)/Gel and Olsa/Gel groups, respectively, nearing the 22.89 g of the normal group. The Cu_2(Olsa)/Gel group also showed a lower disease activity index (DAI) and spleen weight compared to other groups, indicating improved health (Fig. 4B, C and 4D). Moreover, the Cu_2(Olsa)/Gel group exhibited a significantly elongated colon length of 8.62 cm versus other groups (Fig. 4E and F), highlighting superior therapeutic efficacy in mitigating colon shortening. In contrast, the colon length (7.01 cm) of the Cu_2(dobp)/Gel group was similar to that of the DSS group, with no significant difference between them. This indicates that the Cu_2(dobp)/Gel group showed a comparable level of ulcerative colitis alleviation to the DSS group, suggesting that the control MOF material did not substantially contribute to the anti-colitis effect.

To explore the immune regulation effect of Cu_2(Olsa)/Gel, spleen weight and the levels of pro-inflammatory cytokines in the inflamed colons were measured. Cu_2(Olsa)/Gel treatment mitigated the increase in spleen weight, indicating the attenuated immune activation. Meanwhile, Cu_2(Olsa)/Gel significantly reduced the levels of NF-κB, pro-inflammatory cytokines including TNF-α, IL-6 and IL-1β (Fig. 4G and H, S18, S19 and Table S1) and augmented the level of anti-inflammatory cytokine IL-10 (Fig. 4I). We also evaluated the activity of malondialdehyde (MDA) that reflects the ROS level and oxidative stress of inflamed colon tissues [34]. As shown in Fig. 4J, in comparison with DSS group, Cu_2(Olsa)/Gel greatly decreased MDA activity in colon tissues, representing a better remission effect. Thereafter, we studied the histological changes in colon tissues to evaluate the therapeutic efficacy. The DSS group exhibited significant colon tissue damage, characterized by disrupted crypt structure (red arrows in Fig. 4K) and reduced goblet cell count, which are responsible for mucus secretion and mucosa protection. In contrast, Cu_2(Olsa)/Gel treatment preserved colon tissue integrity and maintained goblet cell count similar to the normal group. Additionally, Cu_2(Olsa)/Gel treatment significantly increased the expression of Zonula occludes-1 (ZO-1) and Occludin-1 (OC-1), crucial proteins involved in tight junction formation between intestinal epithelial cells and regulation of intestinal barrier permeability (Fig. 4K and S21). These findings indicated that Cu_2(Olsa)/Gel treatment effectively restored intestinal epithelial barrier function, which is essential for preventing bacterial translocation and inflammation.

Dysbiosis of intestinal microbiota is also closely associated with the development of UC and DSS-induced colitis model [35]. We next examined the gut microbiome changes by 16S ribosomal RNA gene sequencing in V3–V4 regions. Obviously, compared with DSS group, Cu_2(Olsa)/Gel augmented the richness and diversity of the gut microbiome from the Chao and Shannon indexes of operational taxonomic unit (OTU) (Fig. 5A and B). Petal diagram of the species composition suggested that Cu_2(Olsa)/Gel increased the richness of gut microbiome and closed to that of normal group (Fig. 5C). At the order level, appropriate *Firmicutes/Bacteroidetes* (F/B) ratio could be a marker of normal intestinal homeostasis [36]. A markedly decreased proportion of *Bacteroidetes* was observed in the DSS group, which indicated the dysbiosis of gut microbiome; in contrast, the proportion of *Bacteroidetes* in Cu_2(Olsa)/Gel group was similar to that in normal group (Fig. 5D), suggesting the positive intestinal flora regulation. As shown in Fig. S22, compared with the normal and Olsa/Gel groups, the abundance of the harmful pathogenic microorganisms including *Proteobacteria* were also sharply decreased in the Cu_2(Olsa)/Gel group [37]. At Genus level, the heatmap of the relative abundance of intestinal microbiome showed that Cu_2(Olsa)/Gel treatment significantly reduced the relative abundance of the *Romboutsia* and *Enterococcus* family, bacteria that worsen glucose metabolism, in colitis mice [38,39]. On the other hand, after Cu_2(Olsa)/Gel treatment, the relative abundance of the *Lachnospiraceae* was increased, which can hydrolyze starches and other sugars to produce butyrate and other short-chain fatty acids (Fig. 5E) [40]. Non-metric multidimensional scaling (NMDS) plots in the unweighted UniFrac distance was further analyzed. The bacterial community structures of Cu_2(Olsa)/Gel-treated mice displayed a similar gut microbiome profile to normal mice but significantly different from the DSS mice (Fig. 5F). Taken together, Cu_2(Olsa)/Gel enabled gut homeostasis remodeling by a combination of repair of intestinal epithelia barrier and restoration of immune and microbiome homeostasis and thereby efficient colitis alleviation.

2.6. In vivo alleviation of DSS-induced acute colitis in rats

We further investigated the therapeutic efficacy of Cu_2(Olsa)/Gel in DSS-colitis rats. Rats were simultaneously treated with 6% DSS and Cu_2(Olsa)/Gel (Fig. 6A). During the treatment period, normal rats experienced a noticeable increase in body weight from 201.16 g to 247.32 g, whereas rats with DSS-induced colitis rats exhibited dramatic weight loss starting from day 6. Following the completion of treatment, the Cu_2(Olsa)/Gel group showed a body weight recovery to 223.56 g, surpassing the initial weight decrease observed in other disease groups. Compared to the DSS group, the Cu_2(Olsa)/Gel group displayed lower disease activity index (DAI) values and longer colon length. Moreover, Cu_2(Olsa)/Gel showed greater colon length recovery compared to Olsa/Gel (Fig. 6B–E). Visual observations of the anus and miniendoscopic colon demonstrated that Cu_2(Olsa)/Gel effectively reduced intestinal bleeding and hematochezia in DSS-insulted rats (Fig. 6F). Both the remission of symptoms and the endoscopic response suggested Cu_2(Olsa)/Gel provided superior induction therapy compared to Olsa/Gel, potentially benefitting from the sustained release and prolonged retention of Olsa by Cu_2(Olsa)/Gel.

The Cu_2(Olsa)/Gel treatment effectively regulated the inflammatory response in the colon tissues of DSS-colitis rats. It significantly decreased the levels of pro-inflammatory cytokines TNF-α and IL-1β (Fig. 6G and H), which are known to contribute to tissue damage and inflammation in ulcerative colitis. Conversely, it increased the level of the anti-inflammatory cytokine IL-10 (Fig. 6I), which promotes tissue repair and resolution of inflammation in ulcerative colitis. Additionally, Fig. 6J and K illustrated that Cu_2(Olsa)/Gel treatment inhibited the activity of myeloperoxidase (MPO), an enzyme associated with oxidative stress, leading to a reduction in malondialdehyde (MDA), a marker of lipid peroxidation and oxidative stress in the colon tissues. These findings demonstrated that Cu_2(Olsa)/Gel effectively modulated the inflammatory response and reduced oxidative stress in DSS-colitis rats. Histological analysis suggested that Cu_2(Olsa)/Gel treatment effectively attenuated DSS-induced colonic damage, inflammatory cell infiltration and crypt disorder in rats (Fig. 6L and S23). Obviously, Cu_2(Olsa)/Gel treatment led to increased expression of ZO-1 and OC-1, exhibiting significantly integrated colonic epithelium and microvilli. Consistent with these findings, Alcian blue staining mucosa images manifested that Cu_2(Olsa)/Gel treatment normalized the numbers of goblet cells and

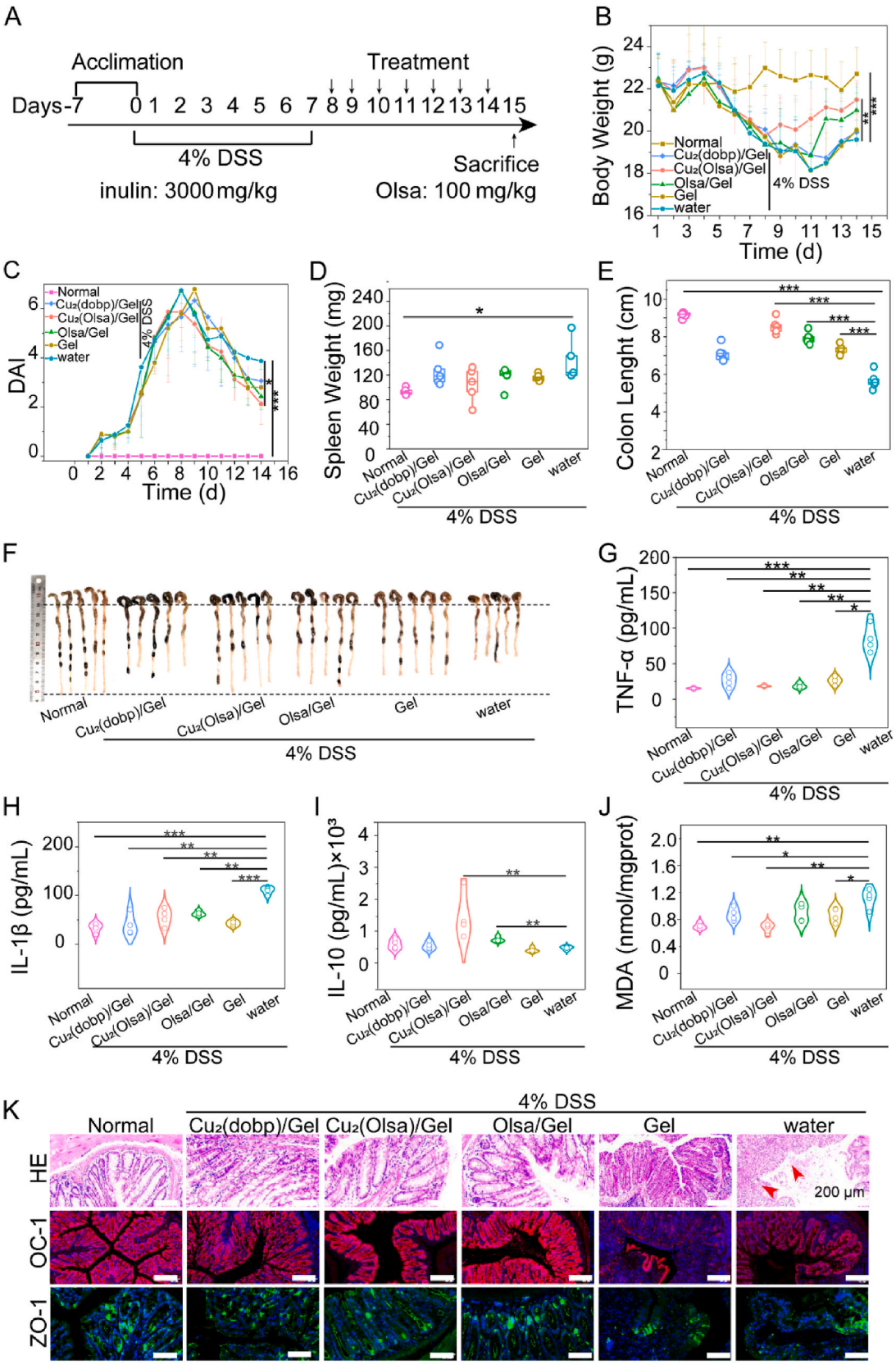

Fig. 4. Therapeutic effect of Cu_2(Olsa)/Gel against DSS-induced UC *via* intragastric administration (i.g.) *in vivo*. (A) Schematic illustration for UC induction and treatment. After provided with water or DSS solution (4%, w/v) for 7 days, mice were intragastric administered with water or various Gels from days 8–14. (B) Body weight changes during the 14-day course. (C) Variations of DAIs. (D) Spleen weight (E) quantified colon length and (F) representative digital photos of colonic tissues isolated from mice after 14 days of treatment ($n = 5$, *p < 0.05, **$p < 0.01$ and ***$p < 0.001$). (G–I) Colonic levels of pro-inflammatory cytokines TNF-α and IL-1β and anti-inflammatory IL-10. (J) Colonic MDA activity ($n = 4$, *$p < 0.05$, **$p < 0.01$ and ***$p < 0.001$). (K) HE staining, ZO-1 and OC-1 immunofluorescence images of the colon tissues (arrowheads: Crypt damage).

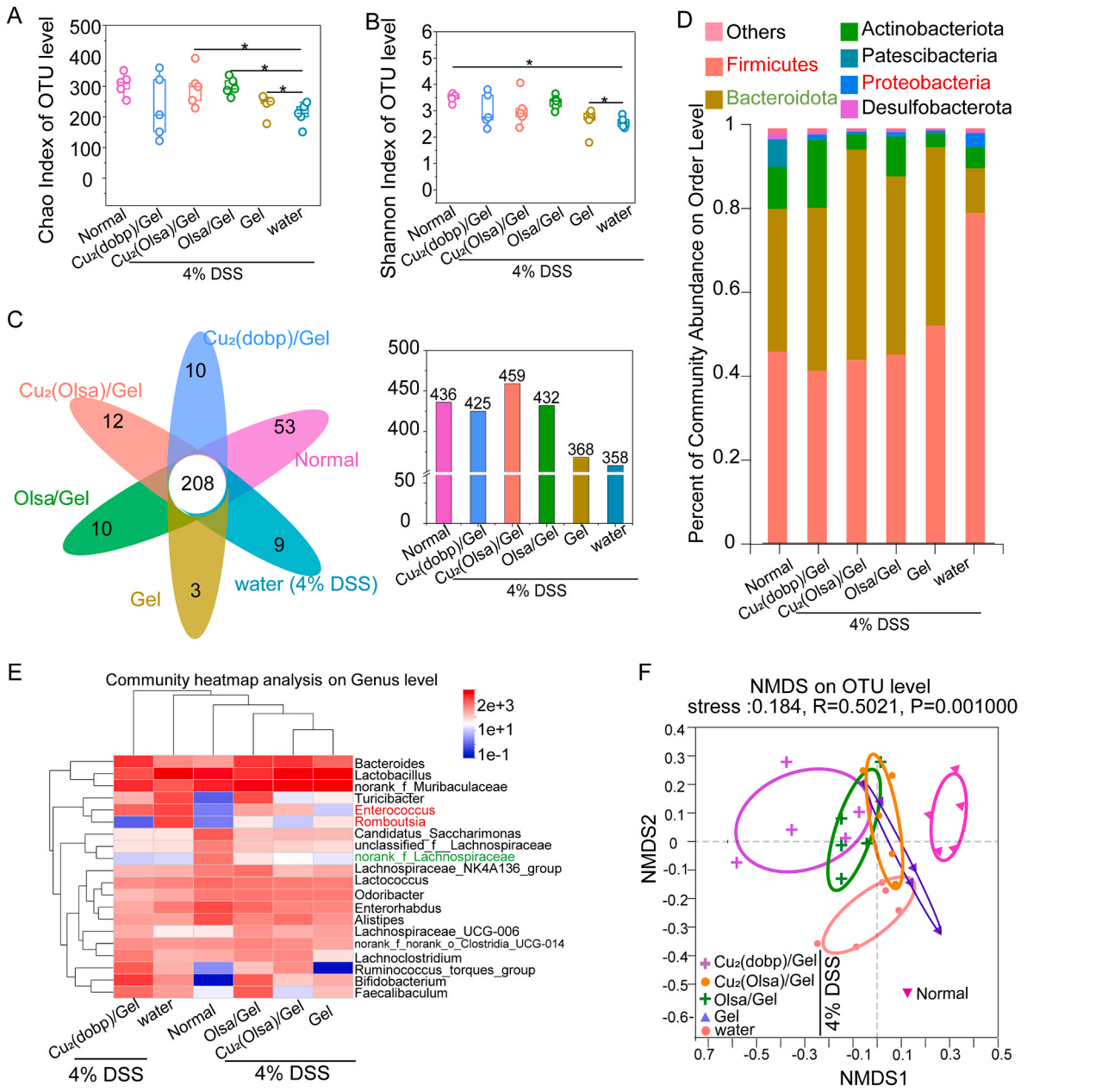

Fig. 5. Cu_2(Olsa)/Gel regulated gut microbiota in DSS-colitis mice. (A) Intestinal communities Chao and (B) Shannon indices of operational taxonomic unit levels (OTU) from different mouse groups. (C) Petal diagram showing intestinal common and unique bacterial species of each group, and histogram showing total number of species in each group at the OTU level. (D) Relative abundances of the intestinal commensal microorganisms at the order levels. (E) Heatmap of the relative abundance of intestinal microbiome at the Genus level. (F) NMDS score plot of β-diversity of the gut microbiota (based on Bray–Curtis).

mucosa thickness (Fig. S24) [41,42]. Furthermore, the HE staining results of major organs revealed negligible organ toxicity or damage (Fig. S25), indicating that these formulations had great biocompatibility. Taken together, our results demonstrated that Cu_2(Olsa)/Gel could achieve restoring the colonic epithelial barrier integrity and retardation of UC progression.

2.7. *In vivo* therapy of TNBS-induced CD mice

The efficacy of different gels against CD was then evaluated by using a TNBS-induced mouse model (Fig. 7A) [43]. As expected, Cu_2(Olsa)/Gel treatment demonstrated superior efficacy in promoting recovery from weight loss (98.1%), reducing DAI value (1.67), and improving colon length (7.82 cm) compared to other treatment groups (Fig. 7B–E). Additionally, the combination of Olsa and inulin gel (Olsa/Gel and Cu_2(Olsa)/Gel) exhibited improved alleviation of inflammation compared to Olsa treatment. Moreover, Cu_2(Olsa)/Gel treatment effectively modulated immune hyper-activation, as indicated by the reduced spleen index (0.33), and balanced pro-inflammatory (TNF-α, 37.55 pg/mL) and anti-inflammatory (IL-10, 405.09 pg/mL) cytokine levels (Fig. 7F–H and Table S2). Histological analysis confirmed that Cu_2(Olsa)/Gel significantly reduced neutrophil infiltration and epithelial damage in the colon tissues. Furthermore, Cu_2(Olsa)/Gel promoted tissue repair and mucus secretion, as observed by improved HE and Alcian blue staining results (Fig. 7I). Cu_2(Olsa)/Gel also enhanced the expression of ZO-1, a tight junction protein responsible for maintaining intestinal barrier function, while inhibiting the activity of MPO, an enzyme associated with oxidative stress and inflammation (Fig. 7I and S26). Collectively, these findings demonstrated that Cu_2(Olsa)/Gel treatment effectively mitigated inflammation, oxidative stress, and

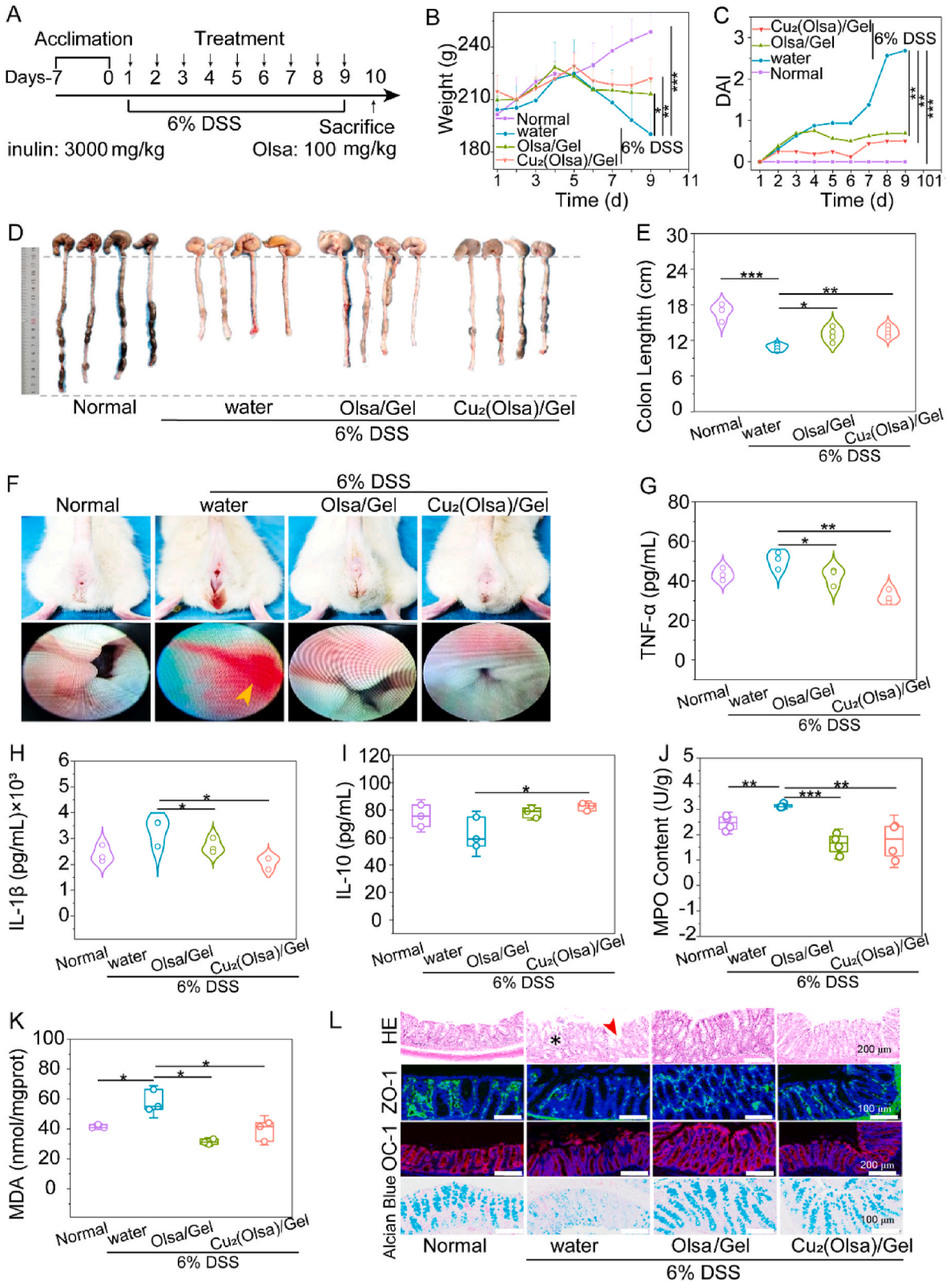

Fig. 6. Therapeutic efficacy of Cu_2(Olsa)/Gel in DSS-induced acute colitis rat. (A) The scheme for DSS treatment and Gels administration. Rats were provided with water or DSS solution (6%, w/v) for 9 days. Variations of the (B) body weight and (C) DAI in the therapeutic period ($n = 4$, $^*p < 0.05$, $^{**}p < 0.01$ and $^{***}p < 0.001$). (D) Representative digital photos of colonic tissues and (E) quantified colon length after 9 days treatment. (F) Representative rats' anus and miniendoscopic images of colons at 9th day (yellow arrow indicated the hemorrhagic spot). (G–I) Colonic levels of TNF-α, IL-1β and IL-10 ($n = 3$, $^*p < 0.05$ and $^{**}p < 0.01$). (J) Colonic MPO contents ($n = 4$, $^{**}p < 0.01$ and $^{***}p < 0.001$). (K) Colonic MDA contents ($n = 3$, $^*p < 0.05$). (L) HE staining, ZO-1, OC-1 immunofluorescence images and Alcian blue-stained mucosa sections of the colon tissues (arrowheads: crypt damage; asterisks: inflammatory cell infiltration).

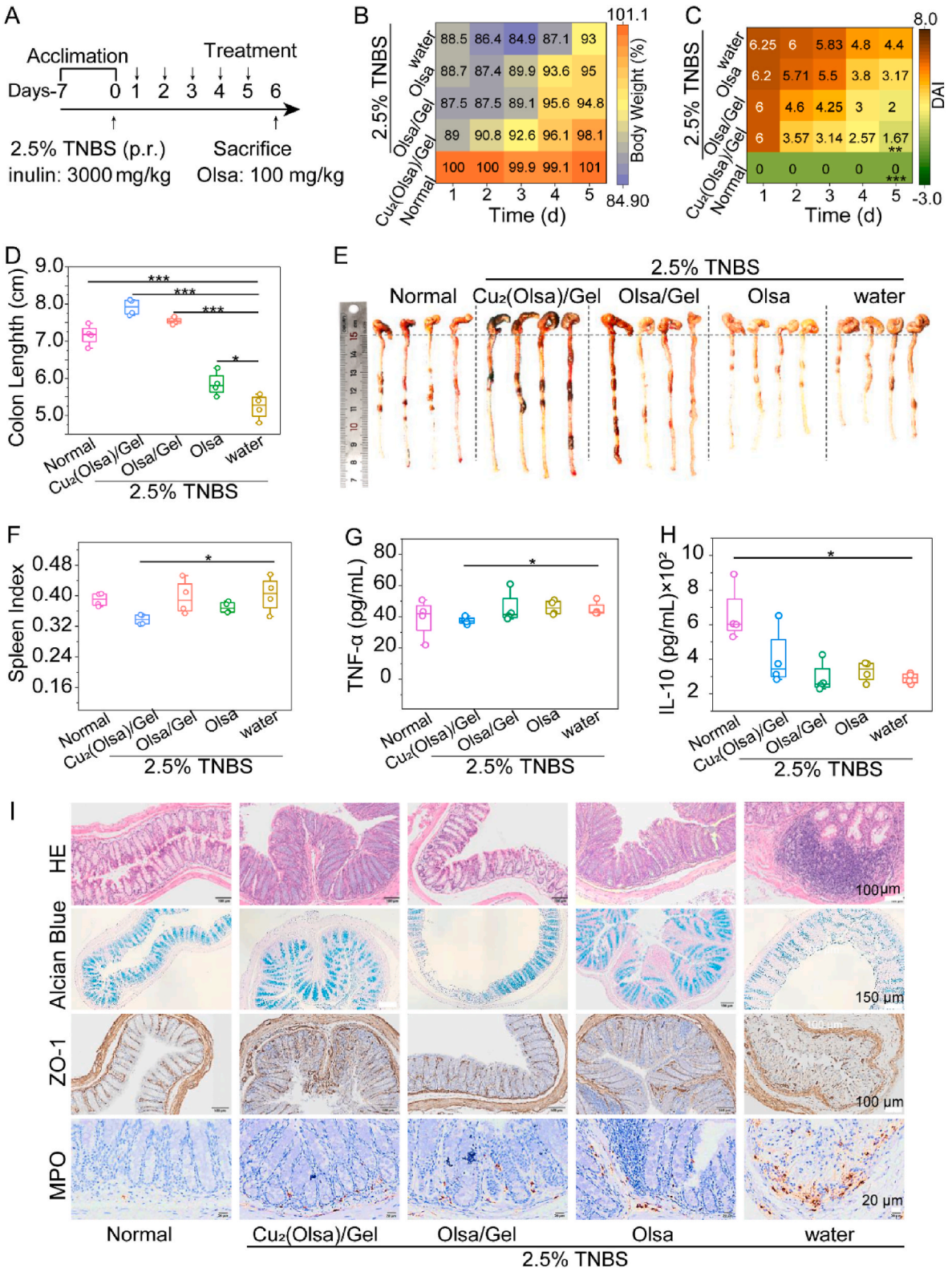

Fig. 7. Therapeutic efficacy of Cu_2(Olsa)/Gel in a TNBS-induced CD mouse model. (A) The scheme for TNBS-induced CD mice and Gels administration. Variations of the (B) mice body weight and (C) DAI during 5 days of treatment ($n = 4$, $^{**}p < 0.01$ and $^{***}p < 0.001$). (D) Quantified colon length and (E) representative digital photos of colonic tissues after 5 days treatment. (F) Spleen index (spleen weight/body weight) of different group ($n = 4$). (G–H) Colonic inflammatory cytokines TNF-α and IL-10 levels. (I) HE staining, Alcian blue-stained mucosa sections, ZO-1 and MPO immunohistochemical images of the colon tissues.

tissue damage, and restored intestinal barrier function in TNBS-mice.

3. Conclusion

In conclusion, we have developed an oral Cu_2(Olsa) nanoneedle-inulin gel composite for the treatment of inflammatory bowel disease. Cu_2(Olsa) was synthesized by a hydrothermal method and its size and morphology could be controlled by adjusting the molar ratios of cupric ions to olsalazine sodium. Cu_2(Olsa) displayed a micron-sized needle-like structure and ROS-scavenging and anti-inflammatory effects. The Cu_2(Olsa)/Gel composite showed sustained drug release in the conditions of gastrointestinal tract and had enhanced bio-adhesion and colonic retention due to its macroporous nature. It improved the function of epithelial barrier by upregulating the expression of tight junction proteins and restored immune homeostasis by balancing pro-inflammatory and anti-inflammatory cytokines and reducing the infiltration of inflammatory immune cells.

Furthermore, the composites had a positive impact on the intestinal microbiome, increasing the abundance of intestinal flora and decreasing the presence of pathogenic bacteria. Thanks to the combinational regulation of intestinal microecology and mucosal barrier, In animal models of colitis induced by DSS and TNBS, Cu_2(Olsa)/Gel composite effectively alleviated colitis symptoms. Importantly, all the ingredients used in the composite are clinically approved or on the GRAS list, ensuring its safety and efficacy as a therapeutic agent. Overall, we provided a biocompatible and economically feasible nanoplatform for reshaping intestinal homeostasis and treating IBD. This nanoplatform could potentially be applied to other medical scenarios where intestinal homeostasis is involved.

4. Methods

4.1. Synthesis of Cu_2(Olsa) MOFs

$CuCl_2$ solution (20 mM, 10 mL) was dropwise added into a solution of olsalazine sodium (10 mM, 10 mL) at a rate of 1 mL/min. The mixture (pH 5.0) was then heated at 30, 50, 70 or 90 °C for 12 h. Then the brown precipitates were centrifuged and washed with water thrice to obtain Cu_2(Olsa). Similarly, Cu_2(Olsa) were prepared by different Cu/Olsa ratios and pHs to obtain the optimal preparation condition. The length and width of MOF were calculated by ImageJ. The dosage of Olsa in supernatant was determined (C1), the production yield of MOF was calculated as follows: Production yield = $(C_0 - C_1)/C_0 \times 100$ (C_0: the initial Olsa dosage).

4.2. In vitro ROS-scavenging of Cu_2(Olsa)

RAW264.7 cells were seeded in 6-well plates at a density of 5×10^4 cells per well and cultured for 24 h. After pre-incubated with Cu_2(Olsa) for 6 h, cells were treated with lipopolysaccharide (LPS, 1 μg/mL) for 2 h. Then the ROS probe, DCFH-DA, was added and intracellular ROS level was determined by CLSM and flow cytometry [44].

4.3. In vitro anti-inflammatory effect of Cu_2(Olsa)

RAW264.7 macrophages were seeded in 24-well plates at a density of 2×10^5 cell per well for 24 h. Then RAW264.7 cells were stimulated with LPS (1 μg/mL) for 4 h after pre-incubation with Cu_2(Olsa) (Olsa: 100 μM) for 12 h. The expression levels of IL-6 related genes were analyzed by real-time reverse transcriptase–polymerase chain reaction (RT-PCR). Total RNA was extracted from cells using RNeasy Plant Mini Kit (Qiagen, Germany). The RNA strand was reverse transcribed into cDNA using the RevertAid First Strand cDNA Synthesis Kit (MBI Fermentas, Germany). The real-time RT-PCR was performed by the StepOne Real-Time PCR System (Applied Biosystems, USA) with KAPA SYBR FAST qPCR Kit (KAPA Biosystems, USA). The gene expression was normalized to β-actin [6].

4.4. Synthesis of Cu_2(Olsa)/Gel

Inulin (200 mg) was dissolved in a suspension of Cu_2(Olsa) (Olsa: 20 mg/mL, 0.3 mL). The mixture was heated to 70 °C for 5 min and cooled at room temperature overnight to obtain Cu_2(Olsa)/Gel [29]. Cu_2(dobp)/Gel and Olsa/Gel were prepared similarly.

4.5. Gastrointestinal tract retention of Cu_2(Olsa)/Gel

All animal studies were performed in accordance with the ethics committee of West China Hospital, Sichuan University. FITC-labeled inulin gel was synthesized according to a previous study [45]. Briefly, to a solution of inulin (2.0 g) and FITC (13 mg) in 8 mL DMSO, $NaHCO_3/Na_2CO_3$ buffer (400 μL) was added and pH was adjusted to 8. After stirring for 24 h, the solution was dialyzed against deionized water to remove free FITC (MWCO 1000 Da). FITC-inulin was obtained after freeze-drying. FITC-tagged inulin gel was prepared as mentioned above by using a mixture of pristine and FITC-labeled inulin at a weight ratio of 5:1.

In vivo retention in DSS-induced UC mice were studied by orally administration with FITC-labeled Cu_2(Olsa)/Gel or Osla/Gel (inulin: 3000 mg/kg, Olsa: 100 mg/kg). At 4, 8, 12 and 24 h post administration, mice were euthanized, the ex vivo fluorescence images of the gastrointestinal tract and main organs were obtained and quantitatively analyzed by an IVIS optical imaging system.

4.6. Treatment of IBD mice

To evaluate the therapeutic efficacy of our material in different aspects of inflammatory bowel disease (IBD), we constructed three animal models, including the two major categories of IBD, ulcerative colitis (UC) and Crohn's disease (CD). The first model was a dextran sulfate sodium (DSS)-induced UC treatment model using mice, which is a widely used model to mimic UC, characterized by superficial mucosal damage and inflammation. The second model was an alleviation UC model using rats, which was designed to facilitate the observation of colonic lesions by colonoscopy and to evaluate the effect of our material on alleviating UC. The third model was a 2,4,6-trinitrobenzenesulfonic acid (TNBS)-induced CD model using mice and rats, which is another commonly used model to mimic CD, characterized by transmural inflammation and ulceration. We used both mice and rats for the TNBS-induced colitis model to demonstrate the reproducibility and robustness of our results in different species.

Treatment of DSS-induced UC Mice: BALB/c male mice (18−20 g) were divided into 6 groups randomly: normal, DSS + water, DSS + Gel, DSS + Olsa/Gel, DSS + Cu_2(Olsa)/Gel, and DSS + Cu_2(dobp). Except for the normal group, other groups involving DSS treatment were first treated with DSS containing drinking water (4%, w/v) for 7 d, and then treated with DSS-free drinking water and orally gavaged with different gels in the following 7 days (inulin: 3000 mg/kg; olsalazine: 100 mg/kg) [29,46]. Weight, visible stool consistency and faeces bleeding were observed and recorded daily. Disease activity index (DAI) is defined as the summation of the stool consistency index (0−3), fecal bleeding index (0−3), and weight loss index (0−4) [47]. On day 15, mice were sacrificed, and the major organs were harvested for histological analysis. The spleen weight was measured. Colonic tissues were imaged and the length was quantitatively analyzed by ImageJ. Then, 1 cm of the distal section was used for histological assessment, including hematoxylin and eosin (HE), ZO-1 and OC-1. Homogenates of the remaining section colonic tissues were taken for measuring the levels of tumor necrosis factor-α (TNF-α), interleukin-10 (IL-10), IL-1β, MPO, and MDA activity by the corresponding commercial assay kits according to the manufactures' protocols [44].

Gut microbiome analysis: To investigate the composition of gut

microbiome in mice, faeces were collected from mice at 15th day. Then 16 S rRNA was used to detect intestinal flora in faece by Shanghai Majorbio Bio-pharm Technology Co., Ltd (Shanghai, China). 338F (5-ACTCCTACGGGAGGCAGCAG- 3) and 806R (5-GGACTACHVGGGTWTCTAAT-3) were chose to amplify this region. First, the whole genome DNA was extracted and amplified; PCR products were quantified and pooled at equimolar amounts. In the end, the completed library was sequenced using an Illumina HiSeq system. Notably, sequencing reads optimized and operational taxonomic unit assigned to taxonomy were basic work before analysis of intestinal microbial community [48].

UC treatment in a retardation model: Male SD rats (~200 g) were divided into 4 groups randomly: normal, DSS + water, DSS + Olsa/Gel and the DSS + Cu_2(Olsa)/Gel. DSS-involved groups were treated with DSS-containing drinking water (6%, w/v) for 9 days and gels were orally administered every day (inulin: 3000 mg/kg; Olsa: 100 mg/kg). On day 10, rats were anesthetized with chloral hydrate and the colonic mucosal damage was observed by an endoscopic video system [47]. Then rats were sacrificed, and the major organs were harvested for histological analysis. Colon tissues and relative inflammatory factors were measured as mentioned section 4.6.

Retardation therapy of TNBS-induced CD Mice: Six-week-old male BALB/c male mice were acclimatized for 1 week. After 12 h of starvation, the mice were injected by 4% chloral hydrate solution to anesthesia. Then 100 μL TNBS (2.5 wt% in 50% ethanol) was administered intrarectally in mice on day 0; normal group mice were received with 50% ethanol alone. After 24 h, water, olsalazine sodium (Olsa), Olsa/Gel, or Cu_2(Olsa)/Gel (inulin: 3000 mg/kg; Olsa: 100 mg/kg) was orally administrated for 5 d. Body weight, visible stool consistency, and faeces bleeding, and DAI values were observed and recorded daily. On day 6, mice were sacrificed, and the major organs were collected for histological analysis. Spleens were weighted and colon lengths were measured. Then, 1 cm of the distal section was used for histological assessment, including hematoxylin and eosin (HE), myeloperoxidase (MPO), malondialdehyde (MDA), zonula occludes (ZO-1) and occludin-1 (OC-1). Homogenates of the remaining section colonic tissues were taken for measuring the levels of tumor necrosis factor-α (TNF-α), interleukin-10 (IL-10) and IL-1β.

4.7. Statistical analysis

All data were expressed as the average ± standard deviation. Statistical comparison between two groups was analyzed by the student's *t*-test. Analysis of variance (ANOVA) was used to compare the differences in different groups, and the data were defined with * $p < 0.05$, ** $p < 0.01$, and *** $p < 0.001$.

Notes

The authors declare no competing financial interest.

Ethics

All animal studies were performed in accordance with the ethics committee of West China Hospital, Sichuan University.

Declaration of competing interest

The authors declare that they do not have any competing interests.

CRediT authorship contribution statement

Zhuangzhuang Zhang: Conceptualization, Data curation, Formal analysis, Investigation, Writing – original draft, Writing – review & editing. **Yang Pan:** Data curation, Formal analysis, Investigation, Methodology, Project administration, Validation. **Zhaoyuan Guo:** Investigation, Methodology. **Xi Fan:** Investigation, Methodology, Validation. **Qingqing Pan:** Investigation, Methodology, Project administration. **Wenxia Gao:** Funding acquisition, Methodology, Supervision, Writing – original draft. **Kui Luo:** Methodology, Resources. **Yuji Pu:** Conceptualization, Formal analysis, Funding acquisition, Investigation, Writing – original draft, Writing – review & editing. **Bin He:** Funding acquisition, Methodology, Resources, Visualization, Writing – original draft, Writing – review & editing.

Acknowledgments

This work was supported by the National Natural Science Foundation of China (51903172, 52073216) and the Sichuan Science and Technology Program (2022NSFSC1939).

Appendix A. Supplementary data

Supplementary data to this article can be found online at https://doi.org/10.1016/j.bioactmat.2023.10.028.

References

[1] R. Ungaro, S. Mehandru, P.B. Allen, L. Peyrin-Biroulet, J.-F. Colombel, Ulcerative colitis, Lancet 389 (10080) (2017) 1756–1770.
[2] K.J. Maloy, F. Powrie, Intestinal homeostasis and its breakdown in inflammatory bowel disease, Nature 474 (7351) (2011) 298–306.
[3] Y. Pu, X. Fan, Z. Zhang, Z. Guo, Q. Pan, W. Gao, K. Luo, B. He, Harnessing polymer-derived drug delivery systems for combating inflammatory bowel disease, J. Contr. Release 354 (2023) 1–18.
[4] Z. Tu, Y. Zhong, H. Hu, D. Shao, R. Haag, M. Schirner, J. Lee, B. Sullenger, K. W. Leong, Design of therapeutic biomaterials to control inflammation, Nat. Rev. Mater. 7 (7) (2022) 557–574.
[5] M. Zu, Y. Ma, B. Cannup, D. Xie, Y. Jung, J. Zhang, C. Yang, F. Gao, D. Merlin, B. Xiao, Oral delivery of natural active small molecules by polymeric nanoparticles for the treatment of inflammatory bowel diseases, Adv. Drug Deliv. Rev. 176 (2021), 113887.
[6] Z. Zeng, X. He, C. Li, S. Lin, H. Chen, L. Liu, X. Feng, Oral delivery of antioxidant enzymes for effective treatment of inflammatory disease, Biomaterials 271 (2021), 120753.
[7] K. Kwon, J. Jung, A. Sahu, G. Tae, Nanoreactor for cascade reaction between SOD and CAT and its tissue regeneration effect, J. Contr. Release 344 (2022) 160–172.
[8] Y. Liu, Y. Cheng, H. Zhang, M. Zhou, Y. Yu, S. Lin, B. Jiang, X. Zhao, L. Miao, C.-W. Wei, Integrated cascade nanozyme catalyzes in vivo ROS scavenging for anti-inflammatory therapy, Sci. Adv. 6 (29) (2020), eabb2695.
[9] J. Xu, J. Xu, T. Shi, Y. Zhang, F. Chen, C. Yang, X. Guo, G. Liu, D. Shao, K.W. Leong, Probiotic-inspired nanomedicine restores intestinal homeostasis in colitis by regulating redox balance, immune responses, and the Gut Microbiome, Adv. Mater. 35 (3) (2023), 2207890.
[10] C. Zhang, H. Wang, X. Yang, Z. Fu, X. Ji, Y. Shi, J. Zhong, W. Hu, Y. Ye, Z. Wang, Oral zero-valent-molybdenum nanodots for inflammatory bowel disease therapy, Sci. Adv. 8 (37) (2022), eabp9882.
[11] J. Liu, Y. Wang, W.J. Heelan, Y. Chen, Z. Li, Q. Hu, Mucoadhesive probiotic backpacks with ROS nanoscavengers enhance the bacteriotherapy for inflammatory bowel diseases, Sci. Adv. 8 (45) (2022), eabp8798.
[12] F. Cao, L. Jin, Y. Gao, Y. Ding, H. Wen, Z. Qian, C. Zhang, L. Hong, H. Yang, J. Zhang, Artificial-enzymes-armed Bifidobacterium longum probiotics for alleviating intestinal inflammation and microbiota dysbiosis, Nat. Nanotechnol. (2023) 1–11.
[13] G. Chen, Y. Yu, X. Fu, G. Wang, Z. Wang, X. Wu, J. Ren, Y. Zhao, Microfluidic encapsulated manganese organic frameworks as enzyme mimetics for inflammatory bowel disease treatment, J. Colloid Interface Sci. 607 (2022) 1382–1390.
[14] S. Zhao, Y. Li, Q. Liu, S. Li, Y. Cheng, C. Cheng, Z. Sun, Y. Du, C.J. Butch, H. Wei, An orally administered CeO_2@montmorillonite nanozyme targets inflammation for inflammatory bowel disease therapy, Adv. Funct. Mater. 30 (45) (2020), 2004692.
[15] J. Liu, L. Shi, Y. Wang, M. Li, C. Zhou, L. Zhang, C. Yao, Y. Yuan, D. Fu, Y. Deng, Ruthenium-based metal-organic framework with reactive oxygen and nitrogen species scavenging activities for alleviating inflammation diseases, Nano Today 47 (2022), 101627.
[16] J.-Y. Lee, R.M. Tsolis, A.J. Bäumler, The microbiome and gut homeostasis, Science 377 (6601) (2022), eabp9960.
[17] J.A. Fitzpatrick, S.L. Melton, C.K. Yao, P.R. Gibson, E.P. Halmos, Dietary management of adults with IBD-the emerging role of dietary therapy, Nat. Rev. Gastroenterol. Hepatol. 19 (10) (2022) 652–669.
[18] M. Wolter, E.T. Grant, M. Boudaud, A. Steimle, G.V. Pereira, E.C. Martens, M. S. Desai, Leveraging diet to engineer the gut microbiome, Nat. Rev. Gastroenterol. Hepatol. 18 (12) (2021) 885–902.
[19] P. Foroozandeh, A.A. Aziz, Insight into cellular uptake and intracellular trafficking of nanoparticles, Nanoscale Res. Lett. 13 (1) (2018) 339.

[20] C.F. Holder, R.E. Schaak, Tutorial on powder X-ray diffraction for characterizing nanoscale materials, ACS Nano 13 (7) (2019) 7359–7365.
[21] P. Guo, H. Song, Y. Liu, C. Wang, $CuFeS_2$ quantum dots anchored in carbon frame: superior lithium storage performance and the study of electrochemical mechanism, ACS Appl. Mater. Interfaces 9 (37) (2017) 31752–31762.
[22] F.E. López-Suárez, A. Bueno-López, M.J. Illán-Gómez, Cu/Al_2O_3 catalysts for soot oxidation: copper loading effect, Appl. Catal., B 84 (3) (2008) 651–658.
[23] W.C. Geng, S. Jia, Z. Zheng, Z. Li, D. Ding, D.S. Guo, A noncovalent fluorescence turn-on strategy for hypoxia imaging, Angew. Chem. Int. Ed. l 58 (8) (2019) 2377–2381.
[24] M.M. Vuolo, V.S. Lima, M.R.M. Junior, Phenolic compounds: structure, classification, and antioxidant power, in: Bioactive Compounds, Elsevier, 2019, pp. 33–50.
[25] T. Liu, B. Xiao, F. Xiang, J. Tan, Z. Chen, X. Zhang, C. Wu, Z. Mao, G. Luo, X. Chen, J. Deng, Ultrasmall copper-based nanoparticles for reactive oxygen species scavenging and alleviation of inflammation related diseases, Nat. Commun. 11 (1) (2020) 2788.
[26] D. Manzanares, V. Ceña, Endocytosis: the nanoparticle and submicron nanocompounds gateway into the cell, Pharmaceutics 12 (4) (2020) 371.
[27] J. Mudter, M.F. Neurath, IL-6 signaling in inflammatory bowel disease: pathophysiological role and clinical relevance, Inflamm. Bowel Dis. 13 (8) (2007) 1016–1023.
[28] Q. Mao, H. Pan, Y. Zhang, Y. Zhang, Q. Zhu, Y. Hong, Z. Huang, Y. Li, X. Feng, Y. Fang, W. Chen, P. Chen, B. Shen, H. Ouyang, Y. Liang, GelNB molecular coating as a biophysical barrier to isolate intestinal irritating metabolites and regulate intestinal microbial homeostasis in the treatment of inflammatory bowel disease, Bioact. Mater. 19 (2023) 251–267.
[29] K. Han, J. Nam, J. Xu, X. Sun, X. Huang, O. Animasahun, A. Achreja, J.H. Jeon, B. Pursley, N. Kamada, G.Y. Chen, D. Nagrath, J.J. Moon, Generation of systemic antitumour immunity via the in situ modulation of the gut microbiome by an orally administered inulin gel, Nat. Biomed. Eng. 5 (11) (2021) 1377–1388.
[30] Y. Guo, de Vasconcelos, L. S, N. Manohar, J. Geng, K.P. Johnston, G.J.A.C. Yu, Highly elastic interconnected porous hydrogels through self-assembled templating for solar water purification, Angew. Chem. 134 (3) (2022), e202114074.
[31] P. Zhao, X. Xia, X. Xu, K.K.C. Leung, A. Rai, Y. Deng, B. Yang, H. Lai, X. Peng, P. Shi, H. Zhang, P.W.Y. Chiu, L. Bian, Nanoparticle-assembled bioadhesive coacervate coating with prolonged gastrointestinal retention for inflammatory bowel disease therapy, Nat. Commun. 12 (1) (2021) 7162.
[32] W. Liang, W. He, R. Huang, Y. Tang, S. Li, B. Zheng, Y. Lin, Y. Lu, H. Wang, D. Wu, Peritoneum-inspired janus porous hydrogel with anti-deformation, anti-adhesion, and pro-healing characteristics for abdominal wall defect treatment, Adv. Mater. 34 (15) (2022), 2108992.
[33] H. Liu, H. Peng, Y. Xin, J. Zhang, Metal–organic frameworks: a universal strategy towards super-elastic hydrogels, Polym. Chem. 10 (18) (2019) 2263–2272.
[34] B. Chami, N.J.J. Martin, J.M. Dennis, P.K. Witting, Myeloperoxidase in the inflamed colon: a novel target for treating inflammatory bowel disease, Arch. Biochem. Biophys. 645 (2018) 61–71.
[35] J.K. Nicholson, E. Holmes, J. Kinross, R. Burcelin, G. Gibson, W. Jia, S. Pettersson, Host-gut microbiota metabolic interactions, Science 336 (6086) (2012) 1262–1267.
[36] S. Stojanov, A. Berlec, B. Štrukelj, The influence of probiotics on the Firmicutes/Bacteroidetes ratio in the treatment of obesity and inflammatory bowel disease, Microorganisms 8 (11) (2020) 1715.
[37] N.-R. Shin, T.W. Whon, J.-W. Bae, Proteobacteria: microbial signature of dysbiosis in gut microbiota, Trends Biotechnol. 33 (9) (2015) 496–503.
[38] R.R. Rodrigues, M. Gurung, Z.P. Li, M. Garcia-Jaramillo, R. Greer, C. Gaulke, F. Bauchinger, H. You, J.W. Pederson, S. Vasquez-Perez, K.D. White, B. Frink, B. Philmus, D.B. Jump, G. Trinchieri, D. Berry, T.J. Sharpton, A. Dzutsev, A. Morgun, N. Shulzhenko, Transkingdom interactions between Lactobacilli and hepatic mitochondria attenuate western diet-induced diabetes, Nat. Commun. 12 (1) (2021) 1–15.
[39] T.J. Fan, L. Goeser, K. Lu, J.J. Faith, J.J. Hansen, Enterococcus faecalis glucosamine metabolism exacerbates experimental colitis, Cell. Mol. Gastroenterol. Hepatol. 12 (4) (2021) 1373–1389.
[40] M.T. Sorbara, E.R. Littmann, E. Fontana, T.U. Moody, C.E. Kohout, M. Gjonbalaj, V. Eaton, R. Seok, I.M. Leiner, E.G. Pamer, Functional and genomic variation between human-derived isolates of Lachnospiraceae reveals inter-and intra-species diversity, Cell Host Microbe 28 (1) (2020) 134–146.
[41] R. Cruz-Acuna, M. Quiros, A.E. Farkas, P.H. Dedhia, S. Huang, D. Siuda, V. Garcia-Hernandez, A.J. Miller, J.R. Spence, A. Nusrat, A.J. Garcia, Synthetic hydrogels for human intestinal organoid generation and colonic wound repair, Nat. Cell Biol. 19 (11) (2017) 1326–1335.
[42] N.G. Kotla, I.L.M. Isa, S. Rasala, S. Demir, R. Singh, B.V. Baby, S.K. Swamy, P. Dockery, V.R. Jala, Y. Rochev, A. Pandit, Modulation of gut barrier functions in ulcerative colitis by hyaluronic acid system, Adv. Sci. 9 (4) (2022), e2103189.
[43] J. Xu, T. Chu, T. Yu, N. Li, C. Wang, C. Li, Y. Zhang, H. Meng, G. Nie, Design of diselenide-bridged hyaluronic acid nano-antioxidant for efficient ROS scavenging to relieve colitis, ACS Nano 16 (8) (2022) 13037–13048.
[44] C. Li, Y. Zhao, J. Cheng, J. Guo, Q. Zhang, X. Zhang, J. Ren, F. Wang, J. Huang, H. Hu, R. Wang, J. Zhang, A proresolving peptide nanotherapy for ste-specific treatment of inflammatory bowel disease by regulating proinflammatory microenvironment and gut microbiota, Adv. Sci. 6 (18) (2019), 1900610.
[45] S. Ohkuma, Use of fluorescein isothiocyanate-dextran to measure proton pumping in lysosomes and related organelles, Methods Enzymol. 174 (1989) 131–154.
[46] H. Sann, J. Erichsen, M. Hessmann, A. Pahl, A. Hoffmeyer, Efficacy of drugs used in the treatment of IBD and combinations thereof in acute DSS-induced colitis in mice, Life Sci. 92 (12) (2013) 708–718.
[47] H.S. Cooper, S.N. Murthy, R.S. Shah, D.J. Sedergran, Clinicopathologic study of dextran sulfate sodium experimental murine colitis, Lab. Invest. 69 (2) (1993) 238–249.
[48] M. Zu, D. Xie, B.S.B. Canup, N. Chen, Y. Wang, R. Sun, Z. Zhang, Y. Fu, F. Dai, B. Xiao, 'Green' nanotherapeutics from tea leaves for orally targeted prevention and alleviation of colon diseases, Biomaterials 279 (2021), 121178.